Journal of Power Sources 241 (2013) 178–185

Contents lists available at SciVerse ScienceDirect

Journal of Power Sources

journal homepage: www.elsevier.com/locate/jpowsour

Analysis of composite electrolytes with sintered reinforcement structure for energy storage applications☆

Sergiy Kalnaus [a,*], Wyatt E. Tenhaeff [a], Jeffrey Sakamoto [b], Adrian S. Sabau [a], Claus Daniel [a,c,d], Nancy J. Dudney [a]

[a] Materials Science and Technology Division, Oak Ridge National Laboratory, Oak Ridge, TN 37831-6083, USA
[b] Department of Materials Science and Engineering, Michigan State University, East Lansing, MI 48824, USA
[c] Energy and Transportation Science Division, Oak Ridge National Laboratory, Oak Ridge, TN 37831-6083, USA
[d] Bredesen Center for Interdisciplinary Research and Graduate Education, University of Tennessee, Knoxville, TN 37996, USA

HIGHLIGHTS

- We study effective conductivity and mechanical properties of composite electrolytes.
- A novel structure with sintered ceramics reinforcement is considered to block Li dendrites.
- Finite element analyses are performed to compute the properties.
- Minimum size of sintering necks necessary to provide desired properties is determined.

ARTICLE INFO

Article history:
Received 15 February 2013
Received in revised form
5 April 2013
Accepted 19 April 2013
Available online 29 April 2013

Keywords:
Lithium ion battery
Composite electrolyte
Sintering
Lithium anode
Dendrites

ABSTRACT

Effective conductivity and mechanical properties of composite polymer electrolytes, in which the reinforcement phase is a sintered packed bed of Li-ion conductive ceramics particles, were estimated using finite element analyses. The computations targeted estimation of the effect of sintering degree, i.e. size of the inter-particle connective necks, on the overall properties of the composite. Methods for microstructure generation and computational procedures were presented. The mechanical ability of the membrane to block lithium dendrites was assessed based on a stability criterion, which depends on the computed effective stiffness. It was found that the minimum size of the inter-particle connections necessary to provide mechanical stability without losing the enhancement in conductivity was 0.05 times the mean particle radius.

1. Introduction

Development of solid electrolytes for electrochemical energy storage devices, such as Li-ion batteries (LIBs), is mainly driven by the flammability concerns associated with the liquid electrolyte compositions, which involve flammable solvents. Improved safety is expected when the thermodynamically unstable and flammable liquid electrolytes are replaced with solid membranes, which in addition to good conductivity would possess adequate mechanical properties to serve as separators between anode and cathode, capable of preventing electrical shorts in a cell caused by formation of lithium dendrites. Finally, stable solid electrolytes are necessary for lithium–air batteries that possess high specific energy density of 11.14 kW h kg^{-1} [1] – close to that of gasoline fuel.

Three general classes of solid electrolytes for LIB applications have been under extensive research – fast ion conducting ceramics, glasses and polymers. In addition, combinations of the above as composite materials have been studied. Ion-conducting ceramics and glasses appear to be promising candidates for solid electrolytes, since they are stable over a wide temperature range. Significant amount of sulfide, oxide and phosphate compounds has been

☆ Notice: This manuscript has been authored by UT-Battelle, LLC under Contract No. DE-AC05-00OR22725 with the U.S. Department of Energy. The United States Government retains, and the publisher, by accepting this submission for publication, acknowledges that the United States Government retains, a nonexclusive, paid-up, irrevocable, worldwide license to publish or reproduce the published form of this submission, or allow others to do so, for United States Government purposes.

* Corresponding author. Tel.: +1 865 576 6181; fax: +1 865 574 4357.
E-mail addresses: kalnauss@ornl.gov, kalnauss2@asme.org (S. Kalnaus).

0378-7753/$ – see front matter © 2013 Elsevier B.V. All rights reserved.
http://dx.doi.org/10.1016/j.jpowsour.2013.04.096

developed, some of which exhibit outstanding ionic conductivity at room temperature. Extensive reviews of available materials can be found in Ref. [2,3]. Sulfide-based conductive glass-ceramics $(1-x)Li_2S-xP_2S_5$ showed room temperature conductivity of ~0.1 S m^{-1} (when $x = 0.2$) – much greater than that of the conductive glass of the same composition [4,5]. Within the group of Li-ion conducting sulfides termed as thio-LISICON (Lithium Superionic CONductor), crystalline $Li_{3.25}Ge_{0.25}P_{0.75}S_4$ has conductivity as high as that of $Li_2S-P_2S_5$ glass-ceramics [6]. Among the phosphates, compounds of sodium conducting NASICON type received most of attention by the researchers with the $Li_{1+x+y}Al_xTi_{2-x}Si_yP_{3-y}O_{12}$ glass-ceramics (LATP) developed by Ohara Inc. showing very high conductivity of 0.12 S m^{-1} at room temperature [1,7,8]. Powders of LATP were mixed with polymer matrix consisting of polyethylene oxide (PEO) and polypropylene oxide (PPO) with LiTFSI ($Li(CF_3SO_2)_2N$) to form a composite electrolyte. The latter was used in a full cell containing $LiCoO_2$ as a positive electrode and $Li_4Ti_5O_{12}$ as a negative electrode, and the cell exhibited good cycling characteristics [7]. In the oxide family, the perovskite Li-ion conductor $Li_{3x}La_{2/3-x}TiO_3$ (LLTO) demonstrated high grain conductivity at $x = 0.125$ [9], the total conductivity however is orders of magnitude lower suggesting the negative influence of grain boundaries [2]. Recently developed oxides with garnet type structure $Li_7La_3Zr_2O_{12}$ (LLZO) can achieve high room temperature conductivities (1×10^{-2} to 1×10^{-1} S m^{-1}) when the cubic phase is stabilized with Al and/or Ta [10,11].

A lithium-ion conductive glass with typical composition $Li_{3.3}PO_{3.8}N_{0.22}$ (LiPON) has been developed at Oak Ridge National Laboratory and has a good lithium conductivity of 2.3×10^{-4} S m^{-1}, and is stable with lithium at high cell voltage [12–14]. Hasegawa et al. demonstrated that LiPON coating of NASICON-type $Li_{1+x+y}Al_xTi_{2-x}Si_yP_{3-y}O_{12}$ (LATP) glass-ceramics electrolyte created the water stable Li/LiPON/LATP system with LiPON serving as a protection from the direct reaction between Li metal and LATP [1].

It should be mentioned that the primary driving force behind the development of solid electrolytes has improvement in ionic conductivity. The importance of mechanical properties, as a part of the overall equation for successful electrolyte, was quantified by Monroe and Newman [15] with the theoretical study of the interplay between shear modulus and compressibility of a material necessary to prevent amplification of non-uniformities on the surface of Li metal anode. Built upon this analysis a mechanical stability criterion was introduced [16]. While Li-ion conductive glasses and ceramics alone are presumed to be stiff enough to prevent lithium dendrite nucleation [17] they are brittle in nature and may not be suitable for applications beyond thin film cells. Polymer electrolytes on the other hand possess very low stiffness but have high degree of incompressibility (resistance to volumetric strain). In addition their conductivity is typically orders of magnitude lower than the conductivity of fast ion conducting ceramics [2]. The combination of the two in form of a composite material should provide adequate mechanical properties and, if formed with the volumetric fraction of ceramics filler being above the percolation threshold, should result in high effective conductivity values. It has been shown, that with the very modest values of Young's modulus of the polymers available for electrolyte applications, the fraction of the ceramics reinforcement should be rather high in order for composite to satisfy the mechanical stability criterion [16]. By introducing polystyrene–polyethylene oxide block copolymers arranged in lamellar structure, polymer electrolytes with excellent conductivity on the order of 3.6×10^{-2} S m^{-1} were obtained, and with increase in PEO molecular weight the improvement in elastic properties was observed [18–20]. The modulus however remained in the range of fractions of 1 GPa, which is much lower than the value needed to stop Li dendrite growth, thus the necessity of reinforcement with a hard phase is still in place. In addition, the contact inter-particle resistance may contribute to lower than expected values of the effective conductivity.

In order to overcome the above limitations, a structure consisting of sintered ceramics ("foam") filled with the polymer is envisioned and is assessed in the current work. With sintered connections between the ceramic particles the additional contact resistance concern is eliminated; the rigid inter-connected ceramic structure would provide appropriate stiffness while mixing with a polymer yields compressibility properties and ductility necessary for mechanical stability. Effective conductivity and mechanical properties were computed based on simulated microstructures with different geometric parameters and different properties of constituents, and the results are discussed in terms of suitability for battery applications. The mechanical stability criterion [16] will be used in current work to estimate the performance of the proposed composite polymer electrolytes (CPEs).

2. Material properties

As a base system a mixture of garnet ceramics [10] and polymer in form of PEO with LiTFSI salt was considered in this paper. The properties of these constituents are listed in Table 1. In the numerical simulations considered, the mechanical properties and conductivity of the ceramics reinforcement phase were kept constant, while the properties of the polymer varied. This was done in order to investigate the influence of polymer properties on overall effective properties of the composite system and screen the possible trade-offs in terms of combination between conductivity and mechanical stability with the lithium metal. It should be mentioned that mechanical properties of PEO available in literature vary by orders of magnitude depending on the measurement technique. Young's modulus of PEO was measured to be 0.2–5 GPa for thin films [21] and 0.29 GPa for highly crystalline bulk material [22]. The Poisson's ratio of PEO was 0.49 [22]. The high value (5 GPa) for the Young's modulus was obtained for thin films using large force indentation experiments [21] and may be relevant to the composites produced by pressing techniques. For PEO nanofibers, Bellan et al. (2005) reported Young's modulus values between 0.5 and 7.0 GPa [23]. The chain Young's modulus of 13 GPa was determined from Raman measurements [24] and can serve as the upper limit of the elastic modulus. Mechanical properties of LLZO ceramics were assumed to be similar to those of Alumina. Conductivity of PEO_{10}:LiTFSI was measured by the authors (Fig. 1) and the results are in agreement with the data available in literature [2,25]. The ionic conductivity of PEO_{10}:LiTFSI was characterized using AC impedance spectroscopy (Solartron 1260). The polymer electrolyte was sandwiched between two parallel stainless steel plates, and the conductivity was calculated using $\sigma = l/RA$, where l is the thickness of the sample, R is the resistance and A is the electrode area.

3. Computational methodology

The computational methodology involves two major steps: (a) microstructure generation, and (b) finite element analysis (FEA).

Table 1
Properties of the constituents (at room temperature).

	σ, S m^{-1}	E, GPa	ν	Ref.
LLZO	4.0×10^{-2}	375	0.22	[11,26]
PEO_{10}:LiTFSI	1.37×10^{-4}	0.29	0.49	[2,22,25]

σ – Ionic conductivity.
E – Elastic modulus.
ν – Poisson's ratio.

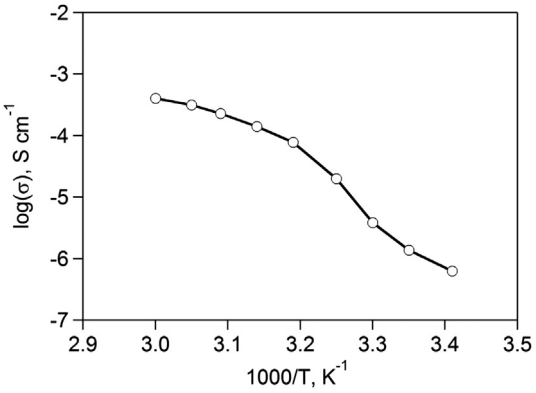

Fig. 1. Conductivity of PEO_{10}:LiTFSI.

The microstructure was generated following the approach previously described in Ref. [27]. Gaussian distribution of ceramics particles (modeled by spheres) with the mean radius of 2 μm and variance of 0.6 μm was chosen to seed the representative volume element (RVE). In order to ensure the contact between the particles necessary for subsequent sintering, a rather high volumetric loading of 52% was simulated, which is close to the random loose packing limit of 55% [28] and apparently much higher than 3D percolation threshold of 30% [29]. Random number generator of Park and Miller [30] was used to prescribe coordinates of the centers of spheres inside RVE and to move them around in order to avoid overlap. The details of the procedure can be found in Ref. [27].

The first step consisted in seeding a relatively large box ($40 \times 40 \times 40$ μm) with the particles from the Gaussian distribution. Then, the central portion ($8 \times 8 \times 8$ μm) of this microstructure was selected with particles contained or intersected by the sides of the cube. This was done in order to completely avoid any edge effects associated with large volume packing. In addition, such reduction in number of particles in RVE was necessitated by the computational limitations and by the complexity of geometry. The resulting RVE contained approximately 13 entire and/or partial particles, which was determined sufficient to obtain reproducible results under subsequent runs with different random seeds.

Sintering between the particles was simulated by creating cylindrical connections, with the central axes of the cylinders aligned with the unit vectors connecting the centers of each pair of particles. The radius was prescribed to be the same for all of the connections and was expressed as a fraction of the mean particle radius ($\rho = r_{neck}/R_{mean}$). By varying the radius of the sintering neck, the effect on the resulting conductivity and mechanical properties was investigated. Examples of microstructures with two different neck sizes are shown in Fig. 2.

The FEA, which was employed to calculate both effective conductivity and elastic mechanical properties, was performed using the COMSOL v.4.3 software. Tetrahedral elements were used and the final mesh contained 70,000 elements. In order to obtain effective conductivity, a constant potential of 5 V was applied to the upper surface of RVE with the bottom surface being ground. The sides of the RVE were prescribed periodic boundary conditions and the equations of electrostatics were solved within the volume. The resulting current density was integrated over the bottom plane of the cube and was used to calculate the conductivity.

FEA has been successfully used to calculate effective elastic mechanical properties of porous ceramic [31], and numerical results were in good agreement with experimental data. In order to compute the effective Young's modulus (E_{eff}) and Poisson's ratio (ν_{eff}), the RVE was subjected to a small (within linear elasticity) strain by application of vertical displacement ($u_3 = -1.0 \times 10^{-10}$ m)

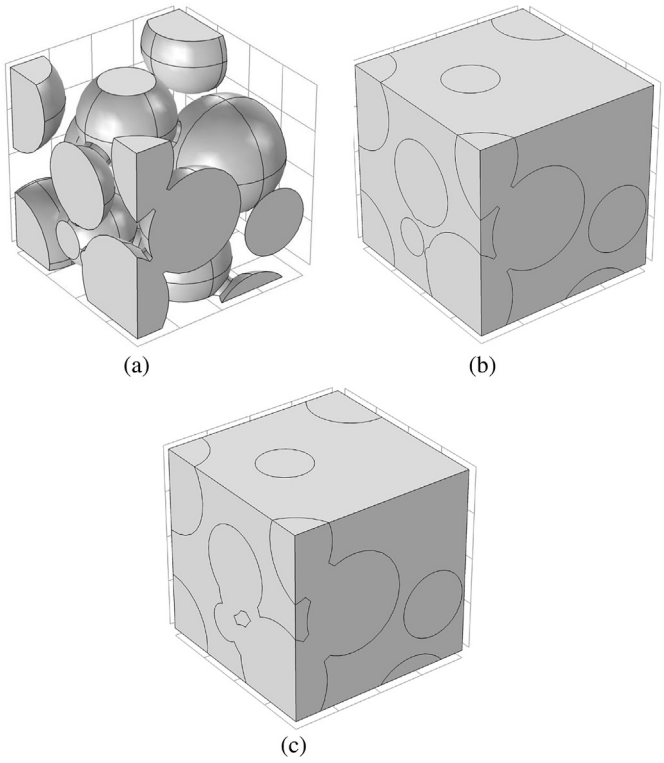

Fig. 2. Simulated microstructure of sintered CPE: (a) connected network of particles within the RVE; (b) complete microstructure filled with polymer, $\rho = 0.3$; (c) complete microstructure filled with polymer $\rho = 0.4$.

to the upper plane. The bottom plane was constrained as $u_3 = 0$ and the remaining sides of the cube were prescribed periodic boundary conditions. After solving the equations of elasticity, the volume-average strains (ε_{ij}) and stresses (σ_{ij}) were determined as [32]

$$\begin{aligned} \langle \varepsilon_{ij} \rangle &= \frac{1}{V} \int_V \varepsilon_{ij} dV \\ \langle \sigma_{ij} \rangle &= \frac{1}{V} \int_V \sigma_{ij} dV \end{aligned} \tag{1}$$

Then the reversed problem was solved to obtain the Young's modulus and Poisson ratio with the assumption of isotropic properties of the composite. This is equivalent to replacing the RVE with the material having equivalent effective properties and matching the resulting stress–strain values.

$$\begin{cases} E_{eff} = \dfrac{\langle \sigma_{11} \rangle (\langle \sigma_{33} \rangle - \langle \sigma_{22} \rangle) + \langle \sigma_{33} \rangle^2 - \langle \sigma_{22} \rangle^2}{\langle \varepsilon_{33} \rangle (\langle \sigma_{11} \rangle + \langle \sigma_{33} \rangle) - \langle \varepsilon_{22} \rangle (\langle \sigma_{11} \rangle + \langle \sigma_{22} \rangle)} \\ \nu_{eff} = \dfrac{\langle \sigma_{22} \rangle \langle \varepsilon_{33} \rangle - \langle \sigma_{33} \rangle \langle \varepsilon_{22} \rangle}{\langle \varepsilon_{33} \rangle (\langle \sigma_{11} \rangle + \langle \sigma_{33} \rangle) - \langle \varepsilon_{22} \rangle (\langle \sigma_{11} \rangle + \langle \sigma_{22} \rangle)} \\ G_{eff} = \dfrac{E_{eff}}{2\left(1 + \nu_{eff}\right)} \end{cases} \tag{2}$$

4. Results

4.1. Effective conductivity

In this section, the influence of the conductivity of the polymer matrix on the overall conductivity of the composite was studied, when the microstructure has geometry beyond the percolation

threshold, that is the majority of the particles are connected together. In this regard we would like to determine the trade-offs associated with lower conductivity of the polymer, approaching the limiting case of virtually non-conductive second phase in the composite. While the initial baseline system consisted of PEO_{10}:LiTFSI matrix ($\sigma_m = 1.37 \times 10^{-4}$ S m^{-1}) and LLZO filler ($\sigma_f = 4.0 \times 10^{-2}$ S m^{-1}), the conductivity of the polymer was varied over the range 1×10^{-10} S m^{-1} to 4.0×10^{-2} S m^{-1} (LLZO conductivity). The results are shown in Fig. 3. The computations were performed for six scenarios corresponding to different radius of the sintering necks connecting the particles, from $\rho = 0.05$ (representing the limiting case of particles brought in contact with each other) to $\rho = 0.4$ (representing well connected network of particles). As it can be seen, the increase in the sintering neck size causes increase in the total conductivity of the composite. An increase in neck radius by a factor of two results in an increase in effective conductivity by a factor of approximately 1.4. The curves corresponding to different neck sizes run parallel to each other within a wide range of polymer conductivity indicating little influence of matrix on the overall behavior of the composite. As the conductivity of matrix increases the curves merge together to the point representing conductivity of LLZO filler.

Such independence of the effective conductivity on the conductivity of polymer matrix is further illustrated in Fig. 4, where all the cases are plotted against the varying neck size. Within the wide conductivity range, the curves corresponding to different polymer conductivities merge together and show the same behavior as a function of the size of sintering connections between particles. When the matrix is resistive compared to the ceramics filler, the major portion of the current is transported via the network of connected particles. This is illustrated in Fig. 5, where the streamlines corresponding to the normalized current density are shown for the case of polymer matrix having the conductivity of 1×10^{-8} S m^{-1}. As conductivity of the matrix increases, both phases start contributing to the current flow thus increasing the total conductivity of the composite. It should be noticed that even when the matrix is resistive, the overall conductivity is higher than that of PEO_{10}:LiTFSI alone. In case of small sintering necks, the resulting value is approximately 3×10^{-3} S m^{-1} which is about 22 times higher than the room temperature conductivity of PEO_{10}:LiTFSI. As the size of the sintering necks becomes larger, an enhancement in the conductivity increases to a factor of 60 compared to the conductivity of the polymer. Results shown in Figs. 3 and 4, indicate that in order to optimize the polymer selection, further efforts may be focused toward selecting the polymer with appropriate mechanical properties, since with percolative network of sintered conductive ceramics particles, the conductivity of polymer plays very little role in the overall behavior.

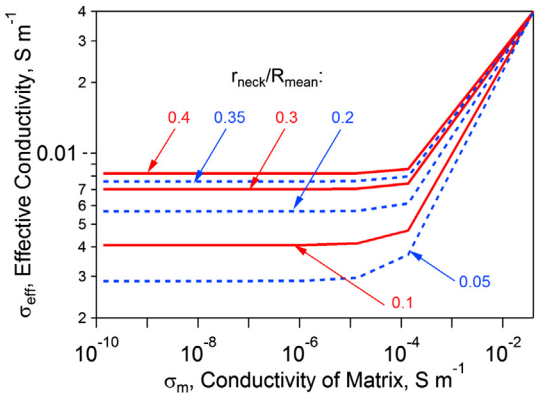

Fig. 3. Effective conductivity as function of the conductivity of the polymer phase.

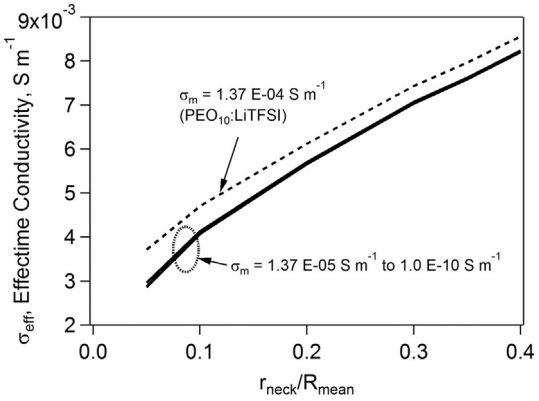

Fig. 4. Effective conductivity as a function of the size of inter-particle connections.

4.2. Mechanical stability

Numerical simulations of the effective mechanical properties were performed by considering that the mechanical properties of the polymer matrix as well as the size of sintering connections between particles vary. Under assumption of isotropic behavior of a particulate composite, the two elastic constants, modulus of elasticity and Poisson's ratio are required to describe the elastic behavior. These were determined from Eqs. (1) and (2), post-processing the results from the FEA. The ability of a composite to suppress Li dendrite formation was evaluated following the analysis by Monroe and Newman [15], where it was postulated that Li surface stability is achieved when the shear modulus of electrolyte would be greater than approximately twice the shear modulus of lithium metal when $\nu_{eff} = 0.33$. This factor-of-two requirement for the ratio of shear moduli gets relaxed when the electrolyte approaches the limit of incompressibility, i.e. when $\nu \to 0.5$. Based on this analysis [15], a stability parameter was introduced in Ref. [16], which incorporates effective shear modulus (G_{eff}) and Poisson's ratio of the electrolyte membrane, and shear modulus of lithium metal (G_{Li}) to form the criterion

$$\xi = \left(a_1 + a_2 \nu_{eff}\right) \frac{G_{Li}}{G_{eff}} \leq 1 \tag{3}$$

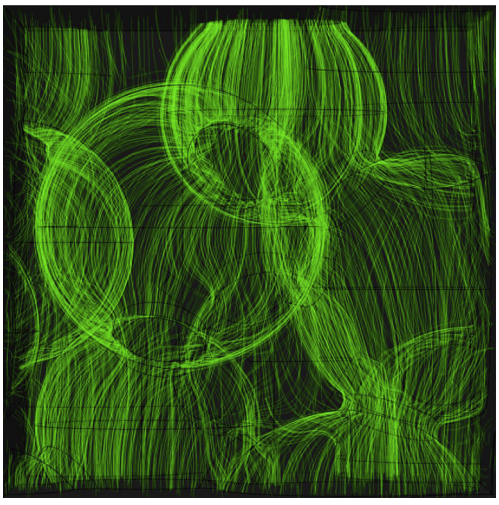

Fig. 5. Current density streamlines in sintered CPE.

where the dimensionless constants a_1 and a_2 were determined to be 3.503 and −5.034 respectively [16]. By means of Eq. (3) the influence of both effective shear modulus and Poisson's ratio is considered in one parameter which aids analysis of the results.

The results of the numerical simulations are shown in Fig. 6. Young's modulus values of the polymer were varied between 0.25 GPa and 6.0 GPa, which reasonably represents the range of values available in literature, excluding the chain modulus of 13 GPa [24]. As can be seen from Fig. 6 the size of the sintering connections between particles plays a major role when the Young's modulus of the polymer is small. As the Young's modulus values increase, the curves corresponding to different radii of inter-particle connections tend to merge together. With the smallest size used in present computations ($\rho = 0.05$) the stability threshold is exceeded, that is when elastic modulus of polymer is 0.25 GPa, the stability parameter is 1.05. All the remaining cases yielded values of ξ well below 1.0 thus indicating mechanical stability of the electrolyte membrane. Neck size of $\rho = 0.05$ therefore can be considered as a threshold for mechanical stability when the volume fraction of ceramics reinforcement is 52%. In the particular case of particle distribution when the mean particle has a radius of 2 μm chosen in our model, this threshold size is 100 nm. However, as the results were represented in a non-dimensional form of the neck size, this threshold can be applied for any other size of ceramics particles.

It should be mentioned that an increase in the value of the stability parameter ξ (that is, a decrease in the mechanical stability of the Li–electrolyte interface) for low-modulus polymers is mostly attributed to the decrease in effective Poisson's ratio, which, for instance in the case of $E = 0.25$ GPa, is equal to 0.17. While the overall stability parameter is still low enough to provide necessary properties for stability, it would be beneficial to have the equivalent Poisson's ratio value closer to that of incompressible material [15]. In this regard, polymers with Young's modulus in the range of 2–3 GPa will yield effective Poisson's ratio close to 0.4, which is beneficial for overall stability.

5. Discussion

Based on the results of the numerical simulations it can be stated that sintered ceramics-based composite electrolytes can create robust structures capable of providing both high conductivity and mechanical properties sufficient for the blockage of Li dendrites. Connecting the particles by sintering provides the necessary stiffness to the structure, as can be seen in Fig. 7, where the distribution of the Von Mises stress in the RVE is shown; the load bearing capability of the composite comes from the connected network of particles that localizes the stress.

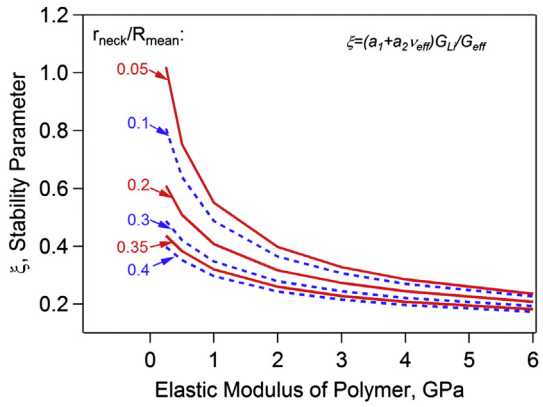

Fig. 6. Stability parameter as a function of elastic modulus of polymer matrix.

Connectivity between particles results in good overall conductivity of the composite (Fig. 3) and avoids issues associated with possible contact resistance between particles in non-connected dispersed systems. As the results suggest, even with small connecting necks between the particles, and highly resistive polymer, the total conductivity remains close to 3×10^{-3} S m^{-1}, which is 22 times higher than the conductivity of the PEO_{10}:LiTFSI polymer alone. This creates the possibility of using stiffer polymers, albeit less conductive or even insulating, to add flexural strength to the composite without sacrificing conductive properties.

The net conduction of Li-ion of the composite structure was estimated by taking into account the lithium transference number of both phases. The cation transference number of Li-conducting ceramics was taken as unity [7,33] and the transference number of the polymer phase was prescribed two limiting values of 0.05 and 0.29 [34,35]. Based on the results from the FEA, the total current passing through each phase was obtained by volume integration over the volume occupied by the phase in the RVE. When normalized with respect to the total current flowing through the RVE, the current fractions can be used to estimate the effective transference number of the composite as

$$t_+ = i_f t_+^{(f)} + i_m t_+^{(m)} \tag{4}$$

where i_f, i_m represent fractions of the total current transferred by the ceramics and polymer phase correspondingly ($i_f + i_m = 1$), and $t_+^{(f)}$, $t_+^{(m)}$ are cation transference numbers of ceramics and polymer electrolytes respectively. The above procedure was applied to the case of dimensionless neck size equal to 0.4 and results are shown in Fig. 8 as a function of conductivity of the polymer electrolyte. As can be seen the results are similar to those obtained for the conductivity (Fig. 3) but demonstrate a trade-off in terms of net lithium conduction when the polymer phase becomes highly conductive. The effective cation transference number remains close to unity when the polymer matrix is resistive enough to restrict the current to flow predominantly through the ceramics phase. It should be mentioned that the above analysis assumes that the transference number of the polymer is constant, equal to the bulk value, and is not changed by the presence of the second phase in the composite structure.

A comparison between the results of FE analysis with predictions based on analytical models applicable to dispersed systems is shown in Fig. 9. Two models were chosen for this purpose – McLachlan's Generalized Effective Medium Theory (GEMT) and Mori–Tanaka model [36–39]. It has been shown that GEMT is applicable without modifications to two-phase particulate composites [36]. Mori–Tanaka model uses Eshelby tensors derived for a particular geometry of an inclusion. The effective moduli produced by Mori–Tanaka approach always satisfy Hashin–Shtrikman bounds for two-phase composites [39]. Both models have analytic formulations, which allow the calculation of the exact solution for effective properties without numerical discretization techniques. Detailed descriptions and derivations of the models as well as formulas for the components of Eshelby tensor for spherical geometry can be found in Refs. [16,36–39]. The same formulations without any modifications were used in current work. The 3D percolation threshold necessary for GEMT was chosen as 0.3 based on a general 3D percolation theory [29].

The results of the FEA of sintered structures are represented in Fig. 9 by two limiting curves – one corresponding to $\rho = 0.05$ (thinnest necks) and one corresponding to $\rho = 0.4$ (thickest necks) in order to simplify the presentation. It can be seen from Fig. 9(a) that the GEMT-based predictions fall within the range of effective conductivity values obtained by finite element analysis. The overall behavior of the effective conductivity as a function of conductivity

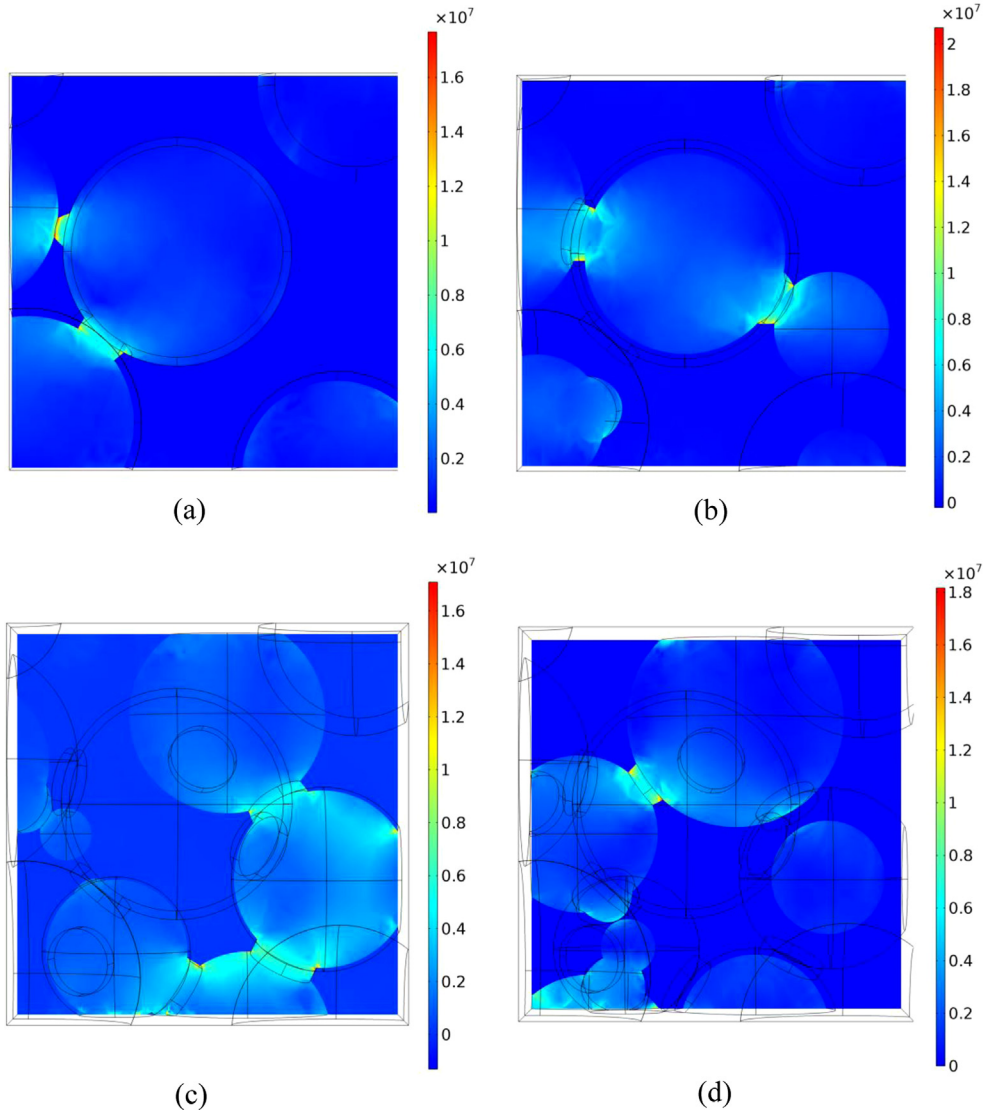

Fig. 7. Vertical slices (*xz*-plane) of the RVE showing the distribution of Von Mises stress at: (a) $y = 7$ μm; (b) $y = 6$ μm; (c) $y = 4$ μm; (d) $y = 3$ μm. The stress color scale is represented in Pa.

of the polymer appears to be the same as in case of FE computations of sintered structures. There is negligible influence of the conductivity of polymer matrix on total composite property when the conductivity of matrix remains low. The effective-medium model however overestimates the effective conductivity compared to the case of $\rho = 0.05$.

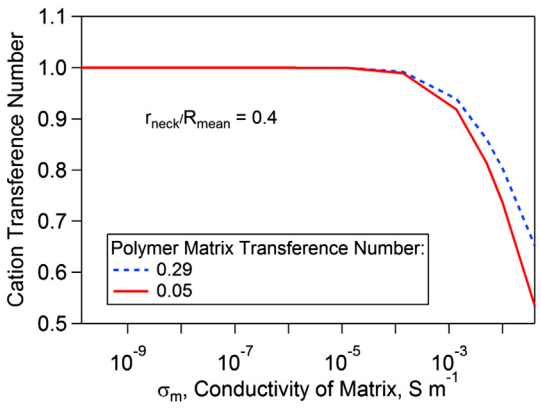

Fig. 8. Cation transference number of the composite electrolyte.

Model of Mori–Tanaka predicts much more unstable material in a sense of mechanical stability with lithium metal (Fig. 9(b)). Since the model describes dispersed systems, connectivity between the particles is not considered which results in lower stiffness and correspondingly higher values of the stability parameter. The latter decreases to the values below 1 (necessary condition for mechanical stability) only when the elastic modulus of a polymer exceeds 2 GPa. At higher values of polymer Young's modulus, the curves corresponding to FEA and analytical model tend to come close to each other. Fig. 8 can serve as an illustration of benefits associated with connecting the particles by sintering, when both the conductivity and mechanical stability are greatly enhanced compared to the dispersed case at the same volume fraction.

Analysis performed by Monroe and Newman [15], from which the stability parameter is derived, makes an assessment of the initiation of Li dendrites based on criterion for amplification of current density at the peaks of surface roughness. For that purpose, a small perturbation of the initially flat interface between lithium metal and polymer membrane is given in the form of $z = A\cos(\omega x)$.

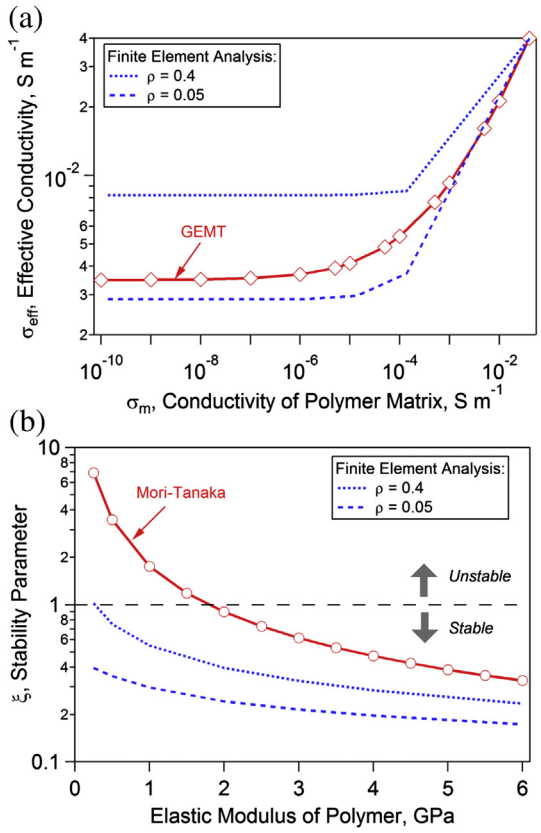

Fig. 9. Comparison between the FEA results and explicit exact solutions obtained with GEMT and Mori–Tanaka models; (a) effective conductivity; (b) mechanical stability parameter.

The resulting elastic displacements are computed and used to obtain the deviatoric and hydrostatic parts of stress tensor via solution of linear elasticity problem with the boundary conditions being zero displacement at $z \to \pm\infty$. These stresses in turn are used to obtain the change in electrochemical potential of electrons within the electrode induced by stress and shape change ($\Delta\mu_{e^-}$). The change in current density is then determined from modified Butler–Volmer equation as

$$\frac{i_\alpha}{i_{\alpha'}} = \exp\left(\frac{(1-c_a)\Delta\mu_{e^-}}{RT}\right) \tag{5}$$

where the subscripts α and α' denote deformed and undeformed states correspondingly. Since the anodic transfer coefficient (c_a) is less than 1, the sign of $\Delta\mu_{e^-}$ determines whether the current is amplified in the deformed state, that is, if $i_\alpha/i_{\alpha'} > 1$ which indicates instability. Through analytical solution of the elastic problem, details of which can be found in Ref. [15], the contributions from the surface tension and mechanical properties of electrolyte to $\Delta\mu_{e^-}$ were determined. It appears that both stresses and surface tension term (which is surface curvature-dependent) are proportional to $A\cos(\omega x)$ and therefore $\Delta\mu_{e^-} \propto A\cos(\omega x)$. The geometrical characteristic of the sinusoidal perturbation is critical, since the solution in Ref. [15] holds only for sufficiently small amplitudes A. Consideration of composite structures would in addition apply a restriction to ω. Since the properties obtained in present study are representative of effective, or homogenized material, the period of the lithium surface perturbation needs to be sufficiently large compared to the particle size; in other words $2\pi/\omega \gg R_{mean}$. While the conclusions in current work are presented in dimensionless form and can be applied to any particle size, consideration of the dimensional relationships presented above indicates the benefit of using smaller particles in CPE so that the material can be approximated as homogeneous within one period of electrode surface roughness wave.

It should be reiterated that all of the results discussed in current work were obtained for a geometry with 52% volume loading of particles which is the random loose packing limit in three dimensions [28]. Theoretically, higher volume fractions of ceramics (possibly at random dense packing limit of 0.64 and even higher for bi-modal particle size distributions) would lead to greater enhancement of both conductivity and mechanical properties. Subsequent filling of the pores with polymer however might present difficulties in manufacturing practice at larger solid loadings. Issues related to the polymer filling can be evaluated by investigating the permeability of the sintered membrane [40]. In cases where polymer filling is difficult, other porous structures, such as ceramic foams would be an acceptable option due to their large modulus at high porosities [40]. We have to mention that other manufacturing possibilities include the cast of a functionally graded ceramic porous membrane, with a continuously increasing mean particle size from top to bottom [41]. Finally, it should be mentioned that grain boundaries created by sintering may contribute to the increase in resistance of the membrane, as has been shown for LLTO ceramics [2,42]. While exceedingly difficult to include in the simulation, comparison of experiment with the simulation should help in extracting the influence of grain boundaries.

6. Conclusions

The finite element analysis of a composite polymer electrolyte performed in the current work shows the interplay between effective conductivity and mechanical properties. A microstructure was considered in which the ceramics phase was sintered and its loading was at values equal to that of the volumetric threshold for loose random packing. The initial properties of constituents were taken as those of LLZO ceramics and PEO_{10}:LiTFSI polymer. Numerical simulations were performed for a range of sizes of the inter-particle connecting necks and for different properties of the polymer filling the space within the ceramics particle network. The ability of such composite membrane to suppress lithium dendrite formation was assessed employing a mechanical stability criterion.

The results suggest that these sintered structures could be successfully used as electrolytes when lithium metal anode is employed. At the lower range of elastic modulus of the polymer, the threshold radius for the sintering connections was determined to be approximately 0.05 times the mean radius of a particle in the composite. For the same dimensionless neck size of 0.05 the overall conductivity was estimated to increase by a factor of 22 compared to PEO_{10}:LiTFSI alone (decreases by 14 times compared to LLZO alone), when the polymer in the composite is highly resistive. This enhancement factor in the conductivity was found to increase with the size of the inter-particle necks.

Acknowledgment

This research at Oak Ridge National Laboratory, managed by UT-Battelle, LLC, for the U.S. Department of Energy under contract DE-AC05-00OR22725, was sponsored by the Vehicle Technologies Program for the Office of Energy Efficiency and Renewable Energy. The seeding algorithm was developed in earlier work sponsored by the Laboratory Directed Research and Development Program (LDRD) of ORNL. Work at Michigan State University was supported by the Office of Naval Research.

References

[1] S. Hasegawa, N. Imanishi, T. Zhang, J. Xie, A. Hirano, Y. Takeda, O. Yamamoto, J. Power Sources 189 (1) (2009) 371–377.
[2] J.W. Fergus, J. Power Sources 195 (15) (2010) 4554–4569.
[3] N.J. Dudney, in: G.-A. Nazri, G. Pistoia (Eds.), Lithium Batteries: Science and Technology, Kluwer Publishing Company, Norwell, Massachusetts, 2004, pp. 623–642. (Chapter 20).
[4] M. Tatsumisago, Solid State Ionics 175 (1–4) (2004) 13–18.
[5] M. Tatsumisago, F. Mizuno, A. Hayashi, J. Power Sources 159 (1) (2006) 193–199.
[6] R. Kanno, M. Maruyama, J. Electrochem. Soc. 148 (7) (2001) A742–A746.
[7] Y. Inda, T. Katoh, M. Baba, J. Power Sources 174 (2) (2007) 741–744.
[8] T. Katoh, Y. Inda, K. Nakajima, R.B. Ye, M. Baba, J. Power Sources 196 (16) (2011) 6877–6880.
[9] J. Ibarra, A. Varez, C. Leon, J. Santamaria, L.M. Torres-Martinez, J. Sanz, Solid State Ionics 134 (3–4) (2000) 219–228.
[10] J.L. Allen, J. Wolfenstine, E. Rangasamy, J. Sakamoto, J. Power Sources 206 (2012) 315–319.
[11] J. Wolfenstine, E. Rangasamy, J.L. Allen, J. Sakamoto, J. Power Sources 208 (2012) 193–196.
[12] J.B. Bates, N.J. Dudney, G.R. Gruzalski, B.A. Zuhr, A. Choudhury, C.F. Luck, J.D. Robertson, Solid State Ionics 53–56 (1992) 647–654.
[13] X. Yu, J.B. Bates, G.E. Jellison Jr., F.X. Hart, J. Electrochem. Soc. 144 (2) (1997) 524–532.
[14] J.B. Bates, N.J. Dudney, B. Neudecker, A. Ueda, C.D. Evans, Solid State Ionics 135 (2000) 33–45.
[15] C. Monroe, J. Newman, J. Electrochem. Soc. 152 (2) (2005) A396–A404.
[16] S. Kalnaus, A.S. Sabau, W.E. Tenhaeff, N.J. Dudney, C. Daniel, J. Power Sources 201 (2012) 280–287.
[17] E. Herbert, W.E. Tenhaeff, N.J. Dudney, G.M. Pharr, Thin Solid Films 520 (1) (2011) 413–418.
[18] M. Singh, O. Odusanya, N.P. Balsara, Nanostructured polymer electrolytes with a high elastic modulus for Li ion batteries, in: 230th National Meeting of the American Chemical Society, Aug 28–Sep 01, Washington, DC, 2005.
[19] M. Singh, O. Odusanya, G.M. Wilmes, H.B. Eitouni, E.D. Gomez, A.J. Patel, V.L. Chen, M.J. Park, P. Fragouli, H. Iatrou, N. Hadjichristidis, D. Cookson, N.P. Balsara, Macromolecules 40 (2007) 4578–4585.
[20] G.M. Stone, S.A. Mullin, A.A. Teran, D.T. Hallinan, A.M. Minor, A. Hexemer, N.P. Balsara, J. Electrochem. Soc. 159 (3) (2012) A222–A227.
[21] H.Y. Nie, M. Motomatsu, W. Mizutani, H. Tokumoto, J. Vac. Sci. Technol. B13 (1995) 1163–1166.
[22] R.W. Warfield, F.R. Barnet, Angew. Makromol. Chem. 27 (410) (1972) 215–217.
[23] L.M. Bellan, J. Kameoka, H.G. Craighead, Nanotechnology 16 (2005) 1095–1099.
[24] K. Song, S. Krimm, J. Polym. Sci. 28 (1990) 63–69.
[25] F. Ren, E.D. Case, A. Morrison, M. Tafesse, M.L. Baumann, Philos. Mag. 89 (14) (2009) 1163–1182.
[26] A. Hekselman, M. Kalita, A. Plewa-Marczewska, G.Z. Zukowska, E. Sasim, W. Wieczorek, M. Siekierski, Electrochim. Acta 55 (2010) 1298–1307.
[27] S. Kalnaus, A.S. Sabau, S. Newman, W.E. Tenhaeff, C. Daniel, N.J. Dudney, Solid State Ionics 199–200 (2011) 44–53.
[28] C. Song, P. Wang, H.A. Makse, Nature 453 (29) (2008) 629–632.
[29] A. Bunde, W. Dieterich, J. Electroceram. 5 (2) (2000) 81–92.
[30] S.K. Park, K.W. Miller, Commun. ACM 31 (10) (1988) 1192–1201.
[31] A.P. Roberts, E.J. Garboczi, J. Am. Ceram. Soc. 83 (12) (2000) 3041–3048.
[32] S.A. Annapragada, D. Sun, S.V. Garimella, Comput. Mater. Sci. 40 (2007) 255–266.
[33] T.M. Arruda, A. Kumar, S.V. Kalinin, S. Jesse, Nano Lett. 11 (2011) 4161–4167.
[34] N. Lu, Y.M. Ho, C.W. Fan, F.M. Wang, J.T. Lee, Solid State Ionics 178 (5–6) (2007) 347–353.
[35] K.E. Thomas, S.E. Sloop, J.B. Kerr, J. Newman, J. Power Sources 89 (2000) 132–138.
[36] D.G. Han, G.M. Choi, Solid State Ionics 106 (1998) 71–87.
[37] Z. Hashin, J. Appl. Mech. 50 (1983) 481–505.
[38] F. Desrumaux, F. Meraghni, M.L. Benzeggagh, J. Compos. Mater. 35 (2001) 603–624.
[39] J.G. Berryman, P.A. Berge, Mech. Mater. 22 (1996) 149–164.
[40] R.A. Lopes, A.M. Segadaes, Mater. Sci. Eng., A 209 (1–2) (1996) 149–155.
[41] K. Darcovich, C.R. Cloutier, J. Am. Ceram. Soc. 82 (1999) 2073–2079.
[42] J. Wolfenstine, J.L. Allen, J. Read, J. Sakamoto, G. Gonalez-Doncel, J. Power Sources 195 (13) (2010) 4124–4128.